Computers and Geotechnics 145 (2022) 104678

Contents lists available at ScienceDirect

Computers and Geotechnics

journal homepage: www.elsevier.com/locate/compgeo

Strain localisation in sensitive clays: can rate dependency provide mesh independent results?

Laura A. Rødvand [a,b,*], Hans Petter Jostad [a], Gustav Grimstad [b], Lars Andresen [a]

[a] Norwegian Geotechnical Institute, Oslo, Norway
[b] Norwegian University of Science and Technology, Trondheim, Norway

ARTICLE INFO

Keywords:
Destructuration
FEA
Regularisation
Shear band
Strain-softening
Structured soil

ABSTRACT

Finite element modelling involving strain-softening materials becomes mesh dependent if not regularised by a mesh independent length scale. The objective of this paper is to investigate whether the inherent strain rate dependency of a sensitive clay can result in mesh independent results in the post-peak strain-softening regime. It describes first a constitutive model that accurately reproduces the rate-dependent behaviour obtained from laboratory tests on block samples of a natural sensitive clay. Then finite element analyses of soil columns under constant shear displacement rate are conducted. The boundaries are closed but internal flow of pore water is allowed. Strain localisation is triggered using a zone with lower undrained shear strength. The results show an interval of regularised strain-softening behaviour before the solution becomes mesh dependent. Pore water flow is found to delay the onset of mesh dependency. In conclusion, this paper achieves a regularised force displacement response for a strain-softening clay, without the need to introduce an artificial internal length scale.

1. Introduction

Rapid loading of soft sensitive clays often results in an undrained or partly drained strain-softening response. In boundary value problems involving such materials this typically results in lower failure loads and often also different failure modes compared to problems involving only perfectly plastic materials. Hence, the capability to reproduce realistic strain-softening characteristics in the material model is necessary for more accurate numerical analyses of engineering problems in sensitive clays. However, numerical analysis of strain-softening materials, using the framework of continuum mechanics and the finite element method, may render a boundary value problem ill-posed, unless an internal length scale is introduced. This can be achieved by using different types of regularisation methods (de Borst et al., 1993). Unless regularised the governing equations lose ellipticity. In a finite element analysis this results in severe mesh dependency due to strain localisation in thin shear bands.

The thickness of shear bands in clay is not well defined. Practically it has proved difficult to measure the evolving shear band thickness from their incipient formation through to the state of global failure and then into the post failure state. For progressive failures such as a slope failure, the failure surface is fully formed and has undergone large displacements before any attempt can be made to measure the shear band thickness. In a laboratory environment it is possible to use digital imagery and software to track displacements (Oka et al., 2005; Thakur et al., 2018), but a shortcoming is that only displacements on the outer surface of a 3D-soil sample are measured. It is also difficult to achieve small enough resolution for clay samples. Based upon special laboratory experiments designed to induce localisation by Gylland et al, 2014 and Thakur et al., 2018, we know that the shear band thickness in sensitive clays evolves during shearing and that at the end of laboratory tests may be in the millimetre scale, however the choice of shear band thickness for finite element analyses remains uncertain.

Modelling the appropriate evolving shear band thickness is crucial to determine the shearing response, load capacity and probably also failure mechanism of localised problems in strain-softening clays. A proper regularisation technique introduces an internal length scale to the constitutive formulation which governs the width of the shearing zone and hence is inevitably linked to the shear band thickness. The non-local strain method has been used as a regularisation method for sensitive clays, but it requires prior knowledge of the shear band thickness and does not account for an evolving shear band thickness through the shearing process.

For materials exhibiting rate dependent behaviour, visco-plasticity is a proven regularisation method for dynamic analyses, but the

* Corresponding author at: NGI, Postboks 3930 Ullevål Stadion, 0806 Oslo, Norway.
E-mail address: laura.rodvand@ngi.no (L.A. Rødvand).

https://doi.org/10.1016/j.compgeo.2022.104678
Received 21 November 2021; Received in revised form 14 February 2022; Accepted 16 February 2022
Available online 8 March 2022

Nomenclature

CSS	current stress surface
D	destructuration parameter
el	element height
G	shear modulus
i	imperfection height
H	column height
ICS	intrinsic compression surface
k	permeability
K	bulk modulus
M	slope of the critical state line
NCS	normal consolidation surface
p'	mean effective stress
p'_{eq}	effective equivalent mean stress
p'_{m}	effective preconsolidation pressure
p'_{mi}	effective intrinsic stress
$p'_{mi,0}$	initial effective intrinsic stress
p'_{0}	initial mean effective stress
q	deviatoric stress
r_{si}	Janbu's creep number
$s_{u,peak}$	peak strength from undrained triaxial experiment
t	time
u	pore pressure
u_x	applied horizontal displacement
y	vertical distance from top of column
β	creep ratio
χ	structure
χ_0	initial value of structure
ε_y	vertical strain
ε^{vp}	viscoplastic strain
ζ	irrecoverable compressibility, $\zeta = \lambda_i^* - \kappa^*$
γ	shear strain
$\dot{\gamma}_a$	applied shear strain rate, $\dot{\gamma}_a = u_x/(H\ t)$
$\dot{\gamma}_i$	shear strain rate in imperfection
$\dot{\gamma}_0$	shear strain rate outside imperfection
κ^*	modified swelling index
λ_i^*	modified compression index for remoulded soil
$d\lambda$	incremental plastic multiplier
$\dot{\lambda}$	plastic multiplier rate
$\dot{\lambda}_{ref}$	plastic multiplier rate at reference state
σ'	effective stress tensor
σ_{xy}	shear stress
σ'_y	effective vertical stress
τ	reference time

regularising effect decreases for slower loading rates (de Borst et al., 1993). For dynamic loading conditions, it has been analytically demonstrated that rate dependency introduces a material length scale (Needleman, 1988; Sluys and de Borst, 1992; de Borst and Duretz, 2020) but it is not possible to do so analytically for quasi-static conditions. Hence, numerical analyses are conducted to assess mesh dependency for quasi-static conditions. Quasi-static conditions are often relevant for engineering problems such as slope stability and bearing capacity. Few studies have been conducted for regularisation of quasi-static clay material by rate dependency. Oka, et al., 1995 present finite element analyses of biaxial compression tests which appear to show limited post peak regularisation, but the results are not conclusive.

A rate dependent formulation is particularly attractive as a regularisation method for soft sensitive clays because these materials display significant strain rate dependent behaviour (Leroueil et al., 1985). Creep models for structured clays have been developed and successfully validated for: laboratory tests with emphasis on 1D compression (Grimstad et al., 2010; Yin and Karstunen, 2011), large-scale embankment tests (Karstunen and Yin, 2010; Rezania, Taiebat and Poletti, 2016), and tunnelling deformations (Tornborg et al., 2021). However, these examples did not involve failure or strain localisation and hence mesh dependency was not examined.

The coupling of pore water flow and effective stresses in finite element analyses can reduce mesh dependency. The soil permeability, hydraulic gradient and loading rate control pore water flow and therefore indirectly establish a weak internal length parameter. Localisation is delayed for dilatant materials (Loret and Prevost, 1991; Schrefler, et al., 1995). For sensitive clays it has been demonstrated that pore water coupling delays the onset of localisation (Jostad, et al., 2006; Thakur, 2011), but alone the process is not enough to prevent mesh dependent results.

This paper proposes the hypothesis that the introduction of a proper rate dependent constitutive formulation in combination with a fully coupled formulation, leads to mesh independent and unique results. Furthermore, that it will provide the information necessary for a realistic representation of an evolving shear band and its thickness.

The aim of this paper is to evaluate the combined effect of strain rate dependency and local pore water flow as a regularisation method for the finite element analysis of soft sensitive clays under quasi-static loading conditions. Specifically; i) to determine if results are mesh independent, ii) to determine if the resulting shear band thickness is independent of element and imperfection size i.e. does the analysis provide an internal length scale.

2. Constitutive soil model and model parameters

2.1. Constitutive model

The applied constitutive soil model is based on the model described in Grimstad et al. (2010) and was implemented as a user defined soil model in PLAXIS 2D 2018 with an implicit backward Euler integration scheme. The model includes a destructuration process and a rate dependency based on the time resistance concept (Janbu, 1985). Anisotropy or stress path dependency has not been included but could be added later.

Three reference surfaces define the model and are illustrated in p'-q space in Fig. 1. The Current Stress Surface (CSS) defines the current stress state and is as per the modified Cam clay model (MCC):

$$p'_{eq} = p' + \frac{q^2}{M^2 p'} \tag{1}$$

where p' is the mean effective stress, q is the deviatoric stress, M is the critical state stress ratio. The CSS represents the intact and bonded clay, whilst the smaller intrinsic surface (ICS) represents the reconstituted soil without any structure. The destructuration process adopts the framework proposed by Gens and Nova, 1993, where the size of the Normal Consolidation Surface (NCS) is a function of the degree of structure, χ, and the size of the ICS, as defined by p'_{mi}, see equation (2). The NCS reduces to the same size as the ICS if the degree of structure is zero. In this way, the ICS represents the remoulded strength of the clay, where sensitivity, $S_t = 1 + \chi_0$, where χ_0 is the initial value of structure.

$$p'_{m} = (1 + \chi) \cdot p'_{mi} \tag{2}$$

A simple destructuration rule causes the NCS to shrink as the plastic strains increase:

$$\frac{d\chi}{d\lambda} = -\chi \cdot D \tag{3}$$

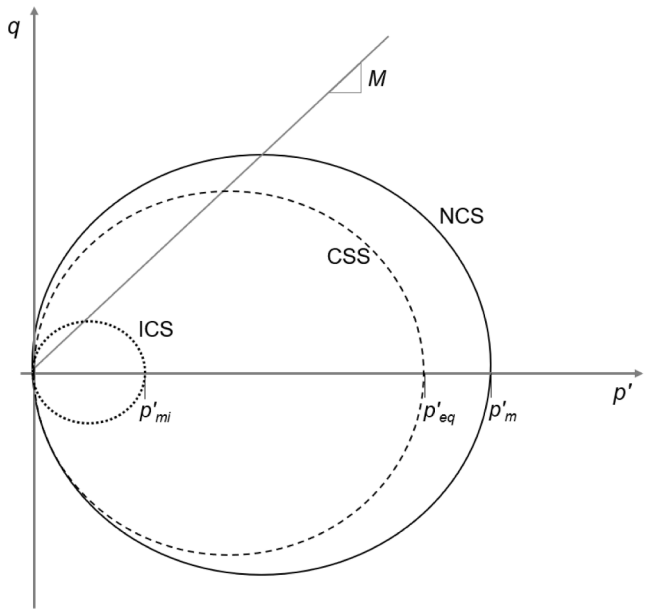

Fig. 1. The reference surfaces in p'-q space: Current Stress Surface (CSS), Normal Consolidation Surface (NCS) and Intrinsic Compression Surface (ICS).

where D is a destructuration parameter. The model assumes an associated flow rule with the plastic potential equal to the CSS, and thus the change in viscoplastic strain ($d\varepsilon^{vp}$) is determined by:

$$d\varepsilon^{vp} = d\lambda \cdot \frac{\delta p'_{eq}}{\delta \boldsymbol{\sigma}'} \tag{4}$$

Rate effects are included though making the plastic multiplier, λ, dependent on time (Grimstad, 2009), as given by:

$$\frac{d\lambda}{dt} = \dot{\lambda} = \dot{\lambda}_{ref} \left(\frac{p'_{eq}}{p'_{m}} \right)^{\beta} \tag{5}$$

where $\dot{\lambda}_{ref}$ is the reference plastic multiplier and β is the creep ratio, which is generally in the range 15–40. Further details on the determination of the rate dependent parameters $\dot{\lambda}_{ref}$ and β may be found in Table 1.

The isotropic hardening rule for the intrinsic reference stress is the same as the Modified Cam Clay model (Schofield and Wroth, 1968):

$$\frac{dp'_{mi}}{d\lambda} = p_{mi} \cdot \frac{1}{\zeta} \cdot \frac{\delta p'_{eq}}{\delta p'} \tag{6}$$

where the hardening parameter, $\zeta = \lambda_i^* - \kappa^*$, and λ_i^* and κ^* are the compression and swelling inclinations in ε_v-ln p' space. The subscript i refers to an intrinsic value for a fully remoulded soil with no structure. A description of all material parameters and how they may be derived is presented in Table 1.

2.2. Input material parameters

The analyses in this paper are based on the behaviour of Tiller quick clay, which is a lightly overconsolidated deposit of very sensitive clay located close to Trondheim, Norway. Additional information on the characterisation and mechanical behaviour of Tiller quick clay may be found in Gylland et al., 2013. Values for input material properties are presented in Table 1. Most input parameters were derived directly from laboratory tests on specimens taken from high quality block samples, with the exception of the destructuration parameter (D) which was fitted to oedometer and triaxial test results. During the calibration of D, it was chosen to prioritise a good fit to the triaxial test because its stress path is more similar to that for the shear column example used later in this paper.

Simulations of an isotropically consolidated undrained compression test (CIUC) and an incrementally loaded (IL) oedometer test are presented in Fig. 2 and Fig. 3 along with the corresponding experimental data. Due to limitations of the constitutive model the simulations do not perfectly replicate the experimental results for both the undrained shear strength and the compressibility whilst using the same set of input material parameters. The use of a more complex destructuration law that defines the proportion of structural degradation caused by plastic deviatoric and plastic volumetric strains, such as that used by (Karstunen et al., 2005) may allow for a better fit, but such a change is expected to have low consequence for the present study.

The destructuration process is depicted in Fig. 4 and occurs most rapidly after exceeding the apparent preconsolidation pressure. The rate of destructuration then decreases as vertical stress increases, until the material is completely remoulded and χ is zero at the intrinsic state.

Other details to note include the choice of stiffness moduli, K and G: the initial stiffness in the simulations is higher than the experimental data. The elastic stiffness moduli were chosen to reflect the unloading stiffness, which is of more importance for the shear strain localisation process. Also, the simulated response of the oedometer shows an almost linear volumetric response after passing the preconsolidation stress. If a higher destructuration parameter were chosen, then the bend in the curve, characteristic to structured soils, would become more visible, but the material response in the CIUC would also become more brittle.

2.3. Rate dependent response

The increase in undrained shear strength of clays with increasing strain rate is well documented (Kulhawy and Mayne, 1990; Soga and

Table 1
Material parameters for constitutive model.

Group	Parameter	Units	Definition	How to determine parameter	Value used for simulations
Standard model parameters	K	kPa	Bulk modulus	–	5000
	G	kPa	Shear modulus	–	5000
	M	–	Slope of the critical state line in p'-q space	Triaxial compression tests	1.5
	ζ	–	$\zeta = \lambda_i^*$- κ^*	From oedometer tests, where λ_i^* is the modified compression index for a remoulded soil, κ^* is the modified swelling index	0.048
Destructuration parameters	χ_0	–	Initial value of structure	From falling cone tests on intact and remoulded clay	99
	D	–	Destructuration parameter	Curve fitting of CRS, IL and CIUC	13
	$p'_{mi,0}$	kPa	Initial size of intrinsic yield surface	From oedometer	1.05
Creep or rate dependency parameters	β	–	Creep ratio = $r_{si} \cdot \zeta$	r_{si} (Janbu's creep number) for fully remoulded soil from IL (Janbu, 1985)	32.5
	$\dot{\lambda}_{ref}$	–	Plastic multiplier at reference state. $\dot{\lambda}_{ref} = 1/(r_{si} \cdot \tau)$ in oedometer conditions. τ = reference time	r_{si} from IL, here τ = 1 day as 24 h IL is used	1.86e-3

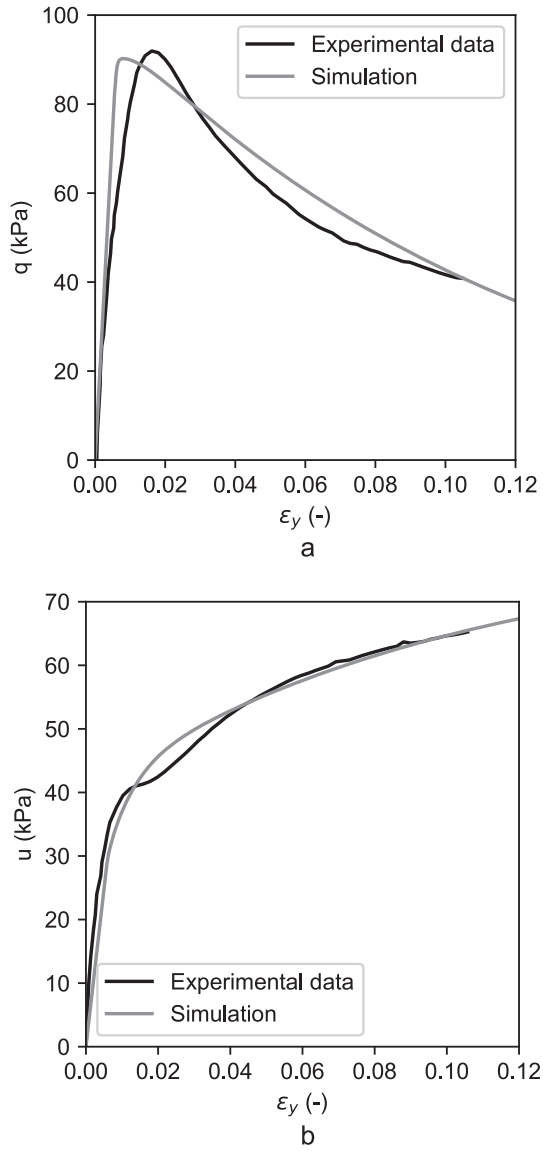

Fig. 2. CIUC 3%/h for a sample from 9.6 m depth. Experimental data versus simulations.

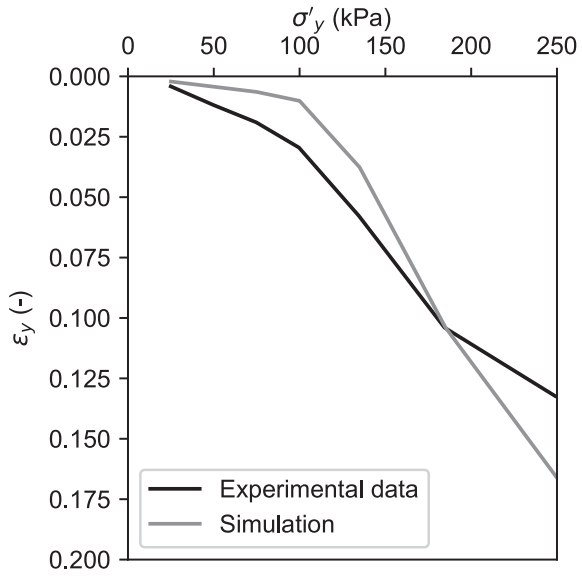

Fig. 3. IL oedometer test for a sample from 9.85 m, with 24 h loading steps. Experimental data versus simulations.

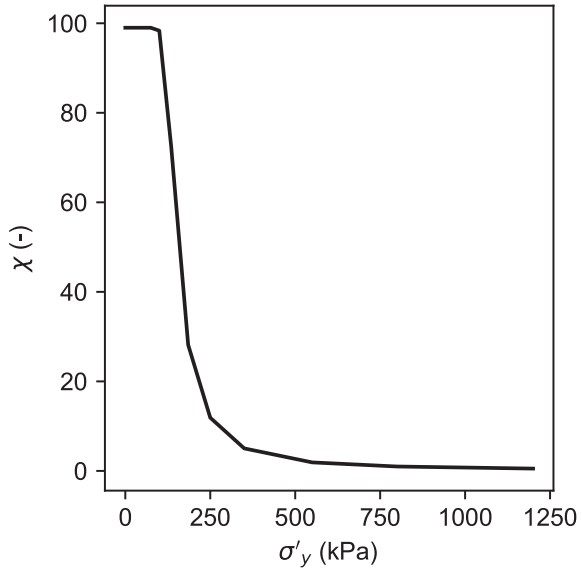

Fig. 4. Simulation of degradation of the soil structure, χ, during IL oedometer test (9.85 m). Data points at end of each 24-hour load step.

Mitchell, 1996; Lunne and Andersen, 2007). This soil model can replicate that same strength increase: see Fig. 5, and the increase per magnitude strain rate is approximately 7 % which is slightly lower than other studies on Tiller clay (Yesuf, 2008; Gylland, et al., 2014).

Structured clays have a unique stress–strain-strain rate relationship as revealed by triaxial tests on non-localised samples by (Berre, 1973; Länsivaara, 1999; Yesuf, 2008). Numerical simulations using the soil model (Fig. 6) also capture this isotach behaviour: for changes in strain rate the stress–strain curve always returns to the corresponding curve for constant rate.

The constitutive model reacts as expected to a change in the applied strain rate. The stress–strain response immediately adapts to the newly applied strain rate: Fig. 6a. Interestingly the stress paths in *p'-q* space (Fig. 6b) deviate further from the constant rate curves: for a large increase in strain rate the clay temporarily dilates, whilst for a decrease in strain rate the stress path drops considerably below the stress path for the constant rate. The stress path returns to the corresponding curve for constant rate, provided enough strain is applied. It should be noted that the rate dependency (absolute in kPa) decreases prior to reaching critical state: the stress paths for constant rates of strain in Fig. 6b converge beneath the critical state line. Also, note the critical state line in *p'-q* space is not rate dependent. This assumption is valid for materials where the interpreted friction angle is unchanged for different strain rates.

In addition to increased undrained shear strength, increasing strain rate will increase the apparent preconsolidation pressure as shown in Fig. 7, this reflects experimental work in sensitive clays by Graham et al. (1983) and Leroueil et al. (1985).

The ability of the model to replicate time dependency in the form of creep and undrained creep failure is also assessed. Fig. 8 demonstrates creep under undrained triaxial boundary conditions. Shear induced pore pressure causes a reduction in effective stresses (stress relaxation) and increases the soil deformation and mobilisation (*q/p'*) at constant shear stress. Highly mobilised soils may creep to failure in a short time (Mitchell and Soga, 2005). Fig. 8a shows that when creep is initiated from higher deviatoric stresses the rate of creep deformation increases, and Fig. 8b demonstrates that the model is capable of reproducing creep acceleration and the development of an undrained creep failure.

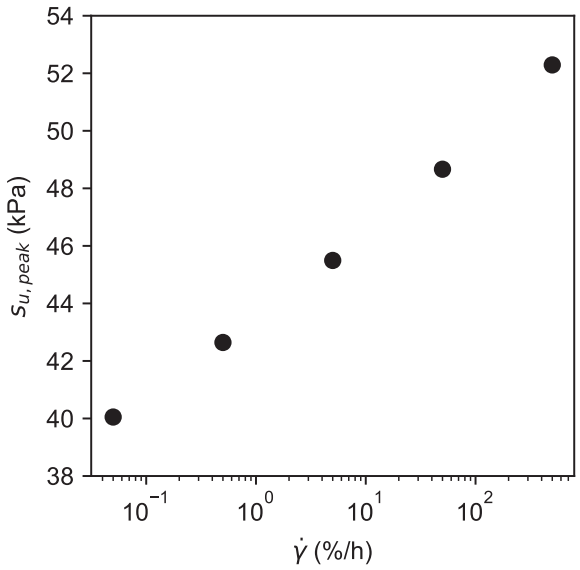

Fig. 5. Effect of strain rate on peak undrained strength, simulated by CIUC strain-controlled element tests.

3. Numerical simulations of shear column

To examine the regularising effect of strain rate dependency in a fully saturated clay a finite element model of a soil column is sheared horizontally. Various changes to the model configuration are applied to assess the mesh dependency of the results and to evaluate the role of rate dependency and pore water flow on the process of shear band generation.

The boundary value problem was chosen specifically to study the shearing behaviour upon the formation of a shear band at macro-scale, such as the conditions in a direct simple shear (DSS) test, hence the model dimensions are at millimetre scale. A one element wide column consisting of 6-noded triangular elements is sheared horizontally, by the application of a displacement u_x at the top of the column (Fig. 9). A constant displacement rate u_x/H is applied during each analysis: also referred to as the applied strain rate ($\dot{\gamma}_a$) in this paper. An initial isotropic effective stress of 100 kPa is applied prior to shearing, and a constant vertical stress of 100 kPa is maintained during shearing. The initial pore water pressure is zero across the full column height. The elements have zero mass to ensure uniform vertical stress conditions within the column.

The base of the column is fully fixed. The nodes on the left and right boundaries are restrained: nodes at the same height can move freely vertically and horizontally but must remain at the same height (tied degrees-of-freedom). This prevents the column from bending and ensures a response comparable to the direct simple shear test (DSS). To replicate an undrained (zero global volume change) test, drainage was not allowed at the boundaries. However, pore water flow is permitted within the column boundaries.

An imperfection is introduced to trigger the strain localisation. The imperfection takes the form of an element cluster with height i in the centre of the column and has a peak undrained shear strength reduction of 0.1 %. Two variations are applied to the imperfection: different imperfection heights, and different discretisation (numbers of elements) are used to test the uniqueness of the solution. The height/width ratio of the elements remains equal to one in all analyses. In later analyses the column height is changed to investigate the role of pore water flow.

The global response is assessed by considering the horizontal force required to maintain the constant applied displacement rate. The results are provided in terms of shear stress (τ) so that different element sizes may be easily compared. The applied horizontal displacement, u_x, is normalised by the column height, H, so that different column heights

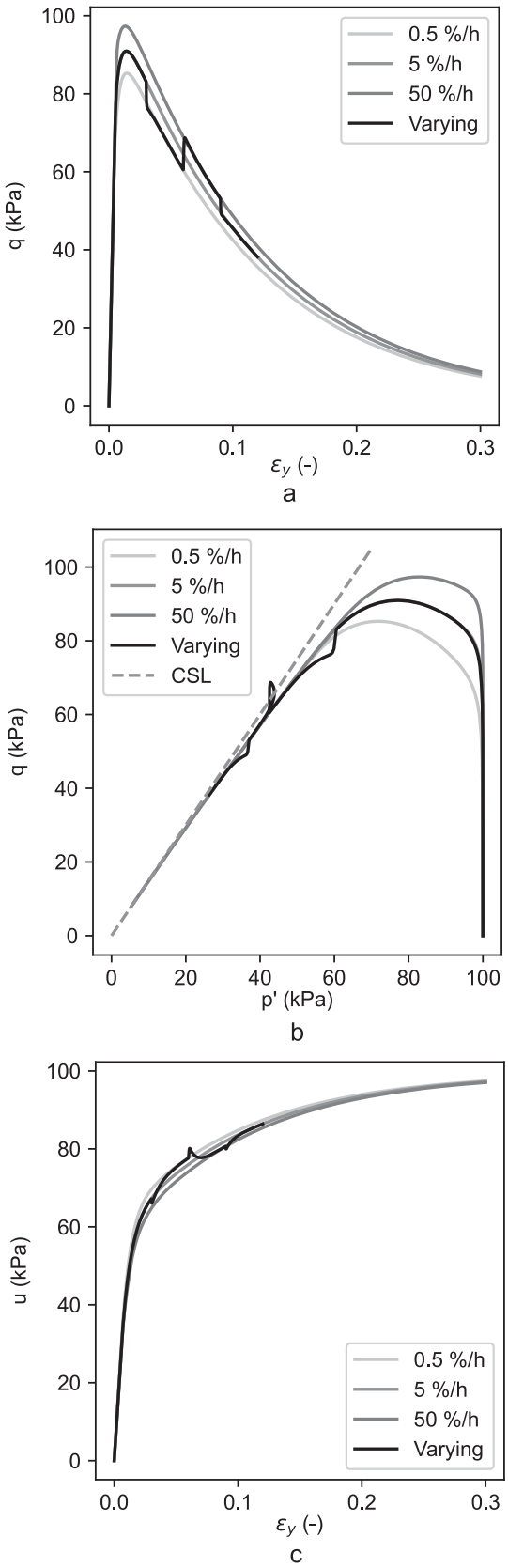

Fig. 6. Effect of changes in applied strain rate on simulated CIUC element tests. One simulation with the strain rate varying between 0.5%/h and 50 %/h.

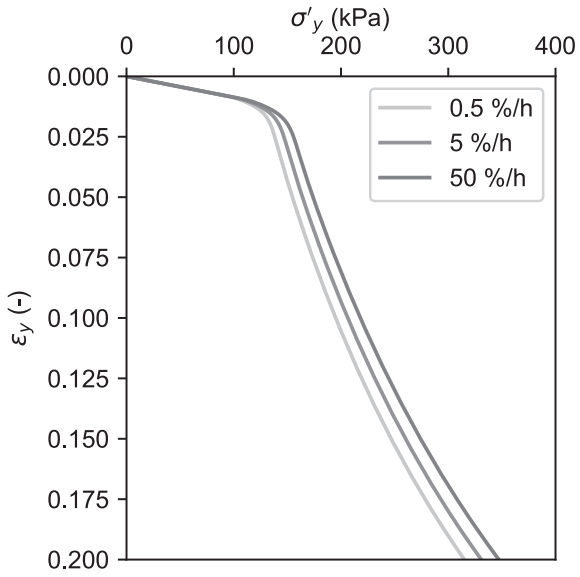

Fig. 7. Simulated Constant Rate of Strain (CRS) oedometer tests, exhibiting rate dependent preconsolidation pressures.

may be compared. The local response experienced in stress points within the column are also presented in the results section: shear strain (γ_{xy}), effective stresses (p', q, σ'_{yy}, σ_{xy}) and pore pressures (u). Following geotechnical convention, compressive stresses and pressures are positive.

During strain-softening the second order work ($W_2^{int} = \frac{1}{2}d\sigma^T d\varepsilon$) is negative. For this paper the definition of the shear band thickness is the height of the strain-softening material i.e. the material with negative second order work. Unloading in the global softening regime is defined by positive second order work. The brittleness of the softening response is defined as the tangential stiffness.

The use of a very small tolerance for the out-of-balance forces is required to capture the latter stages of the strain softening response. It will be shown that large accelerations in shear strain occur toward the end of analyses. For this reason, the analyses are stopped when the element strain rate is greater than 1000 %/h. Stopping analyses at 1000 %/h has no effect on the conclusions.

4. Results

4.1. Mesh dependency

Use of the considered soil model resulted in a period of mesh-independent post-peak softening response. The global softening response consisted of three stages, henceforth termed softening stages, with different degrees of brittleness as shown in Fig. 10. Mesh sensitivity was assessed by using different element sizes: the global response in the first and second softening stages are alike and hence mesh independent. The third softening stage was dependent upon the element height, where a smaller element height resulted in a more brittle response. The detailed material response within each softening stage will be presented in the following sections, but a short definition of the softening stages is provided here for clarity; during softening stage one the deformation is almost uniform across the full height of the column. In stage two softening, unloading occurs outside the imperfection. Finally, in stage three unloading occurs in the imperfection and strain localises in the centre element.

When the height of the imperfection, i, is changed, softening stage two is affected: a smaller imperfection height results in a more brittle global response (Fig. 11). Hence although stage two is mesh independent (Fig. 10), the imperfection height acts as a scaling parameter and plays a role in the response during stage two softening.

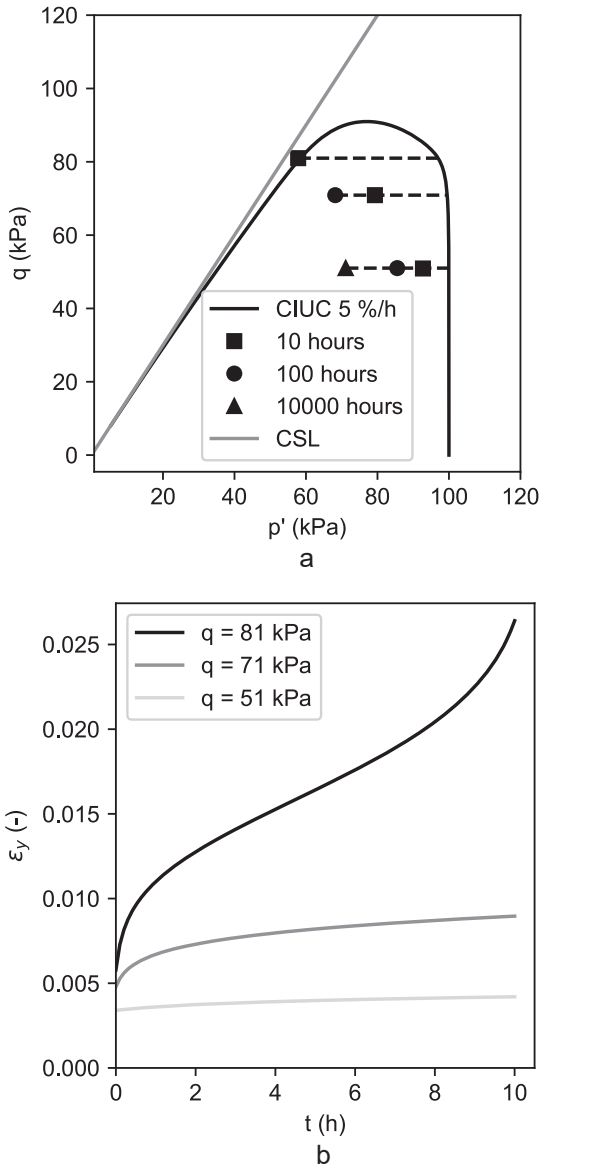

Fig. 8. Simulations of undrained creep tests commencing at different deviatoric stresses: a) stress paths, b) development of strain during 10 h of creep.

4.2. Shear band thickness

Negative second order work, W_2^{int}, indicates the occurrence of strain-softening, and thus was used to determine the shear band thickness during analyses. The stresses and strains used to calculate the second order work were obtained from a vertical section through the column (by using the cross-section tool in PLAXIS), rather than at individual stress points. The stress and strain values were interpolated between stress points. Results show that during stage one softening (Fig. 12a) there was negative second order work over the entire column height, hence the shear band thickness was equal to the full column height, H. During stage two softening (Fig. 12b), the material outside the imperfection experienced positive second order work (was unloaded) and the shear band thickness was therefore equal to the imperfection height. During stage three softening, some positive second order work (unloading) started to develop from the edges of the imperfection (Fig. 12c) and thereafter the thickness of the shear band rapidly reduced.

A consequence of the softening stages definitions is that when

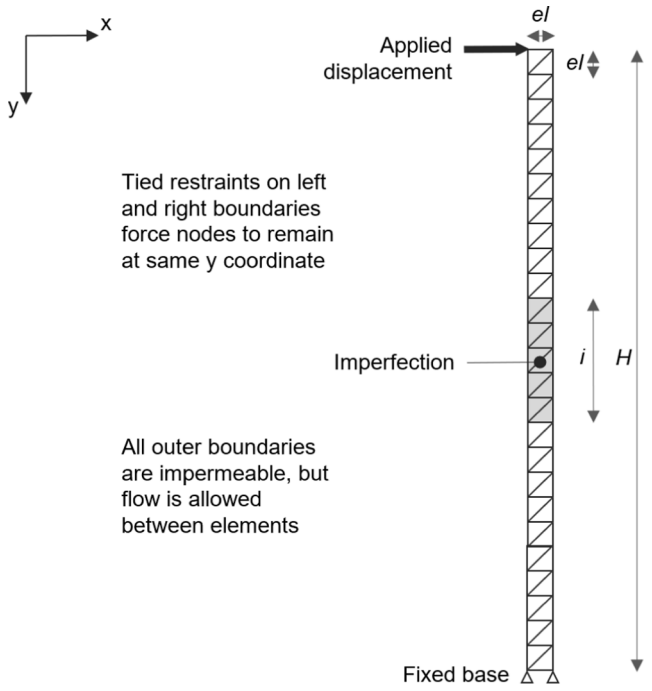

Fig. 9. Finite element mesh and boundary conditions.

assessing: i) different imperfection sizes for softening stage two, or ii) different element sizes for softening stage three, that the end of stages are not absolute and will occur at different u_x/H. Hence the transition between softening stages is a zone rather than a single point in u_x/H.

4.3. Local response

The detailed response of a single column analysis is presented here to explain the mechanisms controlling the global response. The processes occurring are representative and apply to other column heights, soil permeabilities and applied strain rates: see the analyses presented in Section 4.4.

The increased brittleness in the global response for stage two softening was caused by all elements outside the imperfection starting to unload. Smaller imperfection ratio heights (i/H) resulted in a more brittle response (Fig. 11) because a higher proportion of the column existed outside the imperfection and hence a larger proportion of the column was unloaded. All stress points outside the imperfection have the same stress–strain response and hence follow the same curve, labelled "outside", in Fig. 13. Stress points within the imperfection have a similar response and follow the same stress–strain curve until the end of stage two softening.

To maintain the applied displacement rate, any increase in strain rate experienced by the imperfection must be balanced by a decrease in strain rate by material outside the imperfection. The change in strain rates are related to the imperfection height by the following relationship (Needleman, 1988):

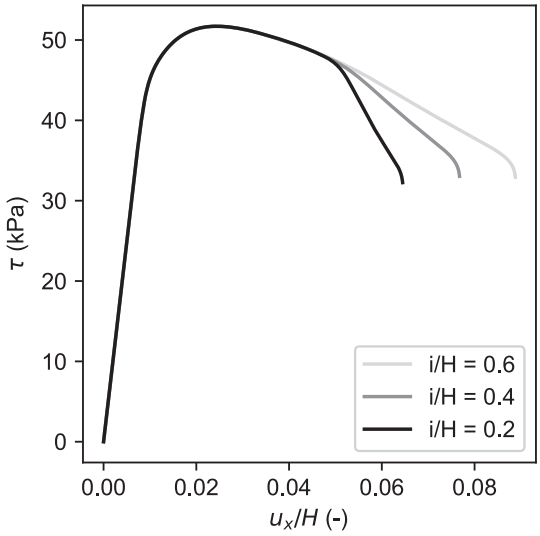

Fig. 11. Effect of changing imperfection size. Global response of a column with H = 10 mm, el/H = 0.002 and $\dot{\gamma}_a$ = 5%/h.

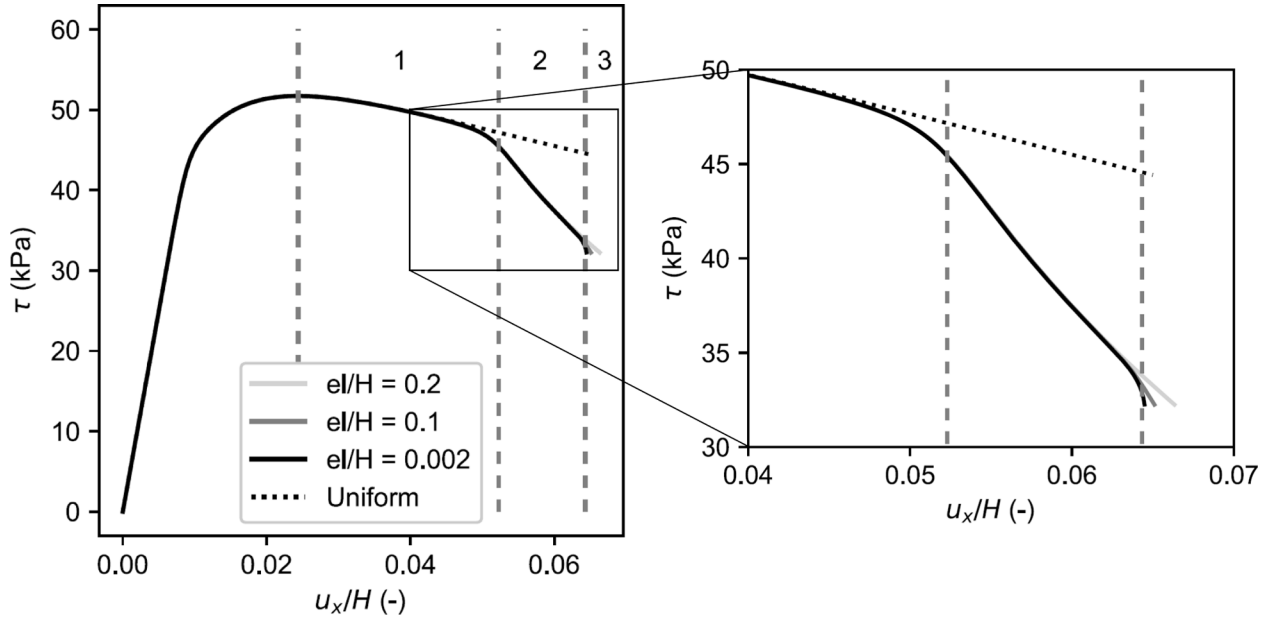

Fig. 10. Mesh sensitivity analysis. Global response of a column with H = 10 mm, i/H = 0.2 and $\dot{\gamma}_a$ = 5 %/h. Dashed lines indicate the start of softening phases 1, 2 and 3. The uniform response represents a non-localised response.

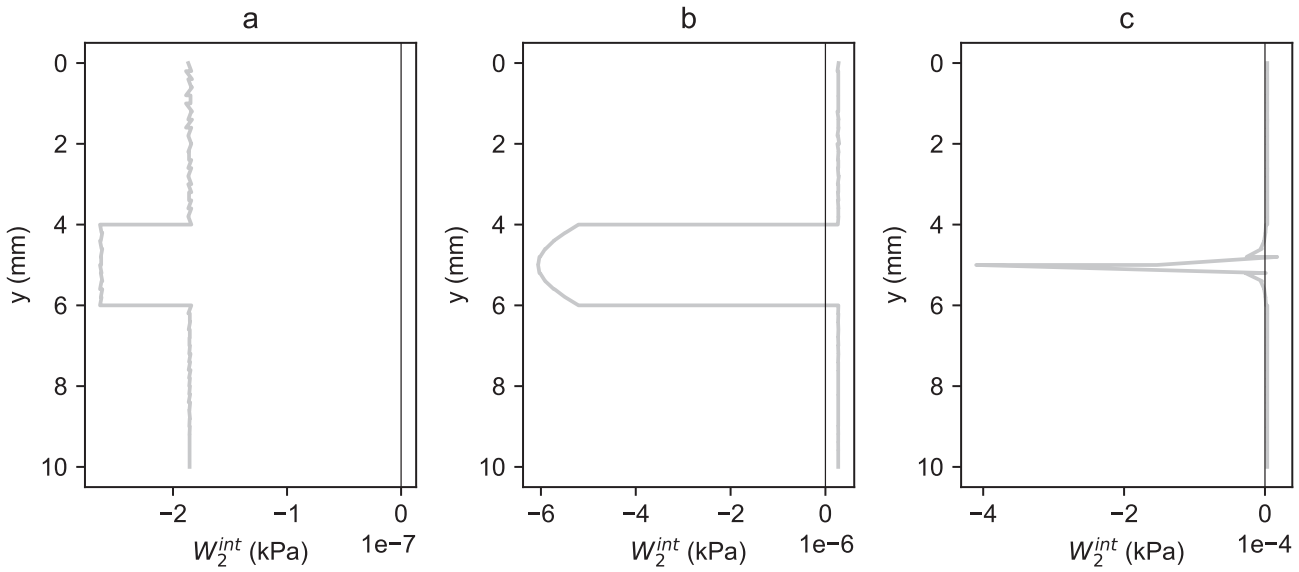

Fig. 12. Second order work at different stages of analysis, where top of column is y = 0 mm and bottom of column = 10 mm: a) stage one softening at $u_x/H = 0.04$, b) stage two softening at $u_x/H = 0.06$, c) stage three softening at $u_x/H = 0.0645$. For H = 10 mm, i/H = 0.2, el/H = 0.02 and $\dot{\gamma}_a$ = 5 %/h.

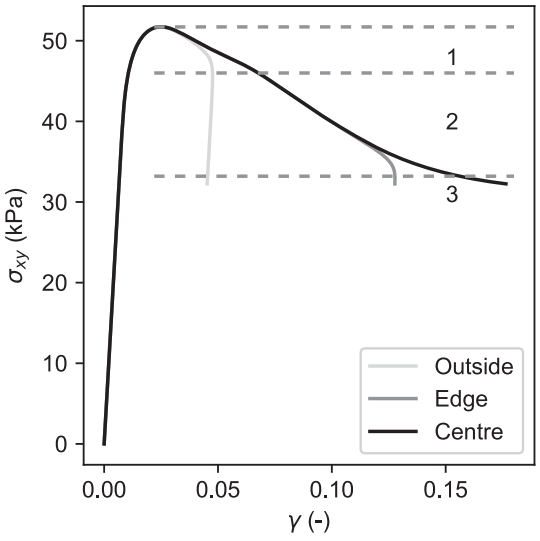

Fig. 13. Local stress–strain responses for material outside imperfection, on edge of imperfection and in centre of imperfection. H = 10 mm, i/H = 0.2, el/H = 0.002 and $\dot{\gamma}_a$ = 5%/h. Dashed lines indicate the start of softening phases 1, 2 and 3.

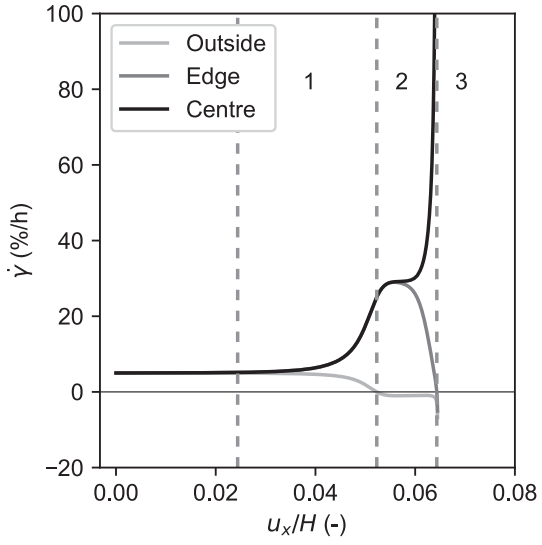

Fig. 14. Local strain rate experienced by material outside imperfection, on edge of imperfection and in centre of imperfection. H = 10 mm, i/H = 0.2 and el/H = 0.002 and $\dot{\gamma}_a$ = 5 %/h. Dashed lines indicate the start of softening phases 1, 2 and 3. Note: strain rate in the plot is limited to + 100 %/h and −20 %/h.

$$\left(1-\frac{i}{H}\right)\cdot\dot{\gamma}_o+\frac{i}{H}\cdot\dot{\gamma}_i=\dot{\gamma}_a \tag{7}$$

where H is the height of the soil column, i is the height of the imperfection, $\dot{\gamma}_i$ is the average shear strain rate experienced by stress points within the imperfection, $\dot{\gamma}_o$ is the shear strain rate experienced by stress points outside the imperfection and $\dot{\gamma}_a$ is the strain rate corresponding to uniform deformation of the column.

All elements outside the imperfection maintained uniform strain rates throughout the analysis, and followed the curve labelled “outside” in Fig. 14. Strain rates within the imperfection remained uniform until mid-stage two, when strain rates became largest in the centre of the imperfection. At the same time the outer edge of the imperfection compensated by decreasing in strain rate. Stage three softening commenced when some unloading also occurred inside the imperfection.

The stress paths in Fig. 15 are presented in both p'-q space and σ'_{yy}-σ_{xy} space due to the model being formulated using invariants (p' and q), whilst σ'_{yy} and σ_{xy} are the stress variables of the problem enforced by equilibrium. Fig. 15a demonstrates that the material outside the imperfection is less mobilised (in q/p') than the material within the imperfection. The stress paths in σ'_{yy}-σ_{xy} space (Fig. 15b) are almost identical due to the requirement for shear and total vertical stress equilibrium across the full column height, and because the pore pressure equalises in the 10 mm column height. The different p' over column height is thus due to variation in σ'_{xx} over the column height.

Due to the small height of this column (10 mm) pore water flow enables pore pressure equalisation in the column for the given permeability: pore pressure at all stress points appear as a single line in Fig. 16. However, it is difficult to determine from this single analysis if the uniform pore pressure is due to different pore pressure generation at different strain rates, or to what extent pore water flow from the shear

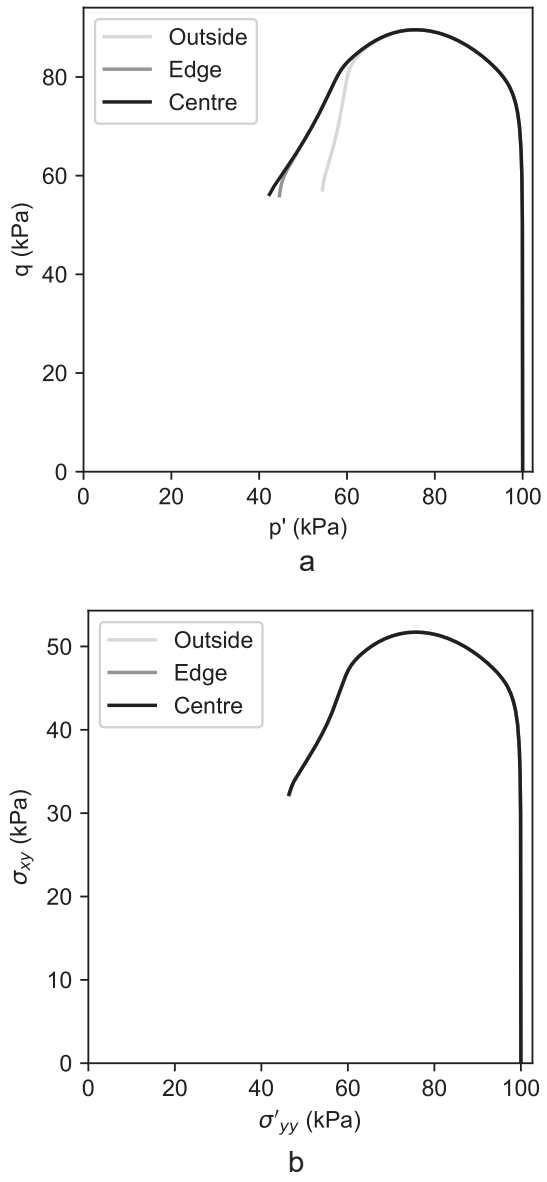

Fig. 15. Stress paths for material outside imperfection, on edge of imperfection and in centre of imperfection. H = 10 mm, i/H = 0.2, el/H = 0.002 and $\dot{\gamma}_a$ = 5 %/h.

band to surrounding material influences the results. The next section will analyse a variety of cases to induce different pore water pressure responses.

4.4. Changing the boundary conditions

To determine the extent of regularising effects due to either strain rate dependency or pore water generation and dissipation, Fig. 17 presents the global response and pore pressure response for analyses with different: i) permeabilities, ii) column heights, iii) applied strain rates. The pore pressure gradient, Δu, is the difference between the excess pore pressure at the centre of the shear band and the top of the column. It is normalised by the initial mean effective stress (p'_0).

The following may be concluded from the results:

- When the same strain rate was applied, stage one softening results were independent of permeability, imperfection height and column height: Fig. 17 a and b.

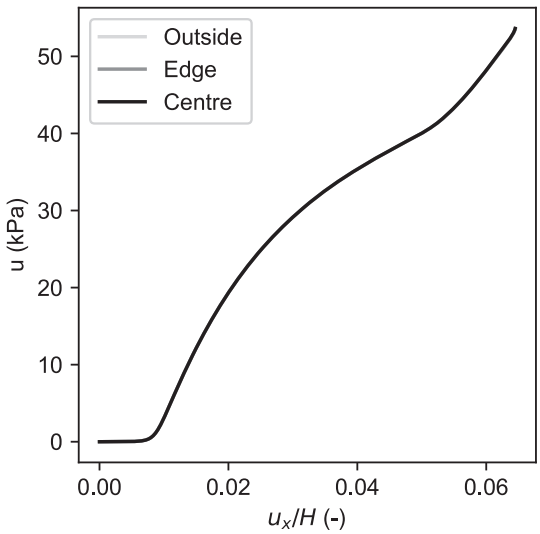

Fig. 16. Local pore pressure response against applied horizontal displacement, u_x/H. For material outside imperfection, on edge of imperfection and in centre of imperfection. H = 10 mm, i/H = 0.2, el/H = 0.002 and $\dot{\gamma}_a$ = 5 %/h.

- The duration of stage two softening was affected by the pore pressure gradient, which in turn was influenced by permeability, imperfection size, column height and applied strain rate.
- Increasing the material permeability extended the duration of stage two softening (Fig. 17a) and allowed better equalisation of pore pressure (Fig. 17d) hence pore water flow assisted the regularisation process.
- When the size of imperfection and column height were changed whilst maintaining the same *i/H* ratio (and hence same local strain rates), the thicker imperfection become mesh dependent first: Fig. 17b. A larger pore pressure gradient developed in the thicker imperfection (Fig. 17d), presumably because the water had a larger distance to flow to reach the unloading material outside the shear band.
- Increasing the applied strain rate provided greater peak strength and a shorter duration of stage two softening: Fig. 17c. Larger pore pressure gradients developed for the faster applied strain rates (Fig. 17f) as the pore water had less time to flow out of the shear band.

5. Discussion

In short, the analyses demonstrate that i) the global softening response consists of three stages with different responses, ii) softening stages one and two are mesh independent, iii) the shear band thickness is equal to the imperfection height during softening stage two, and iv) once some material in the imperfection starts to unload during softening stage three, the shear band thickness rapidly reduces to the height of a single element. This section provides some detailed discussion on the causes for the observed response.

5.1. Rate dependent response

5.1.1. Unique solution

A regularised solution occurs because all strains are prevented from instantaneously transferring to a single element. A large increase in the strain rate inside the shear band would result in an increase in the shear stress, which would be in contradiction to the shear stress decrease for unloading material outside the shear band, or for the decreasing strain rate at the edge of the shear band. The same shear strength reduction must occur both inside and outside the imperfection to maintain equilibrium (uniform shear stress over the entire column height). Only one

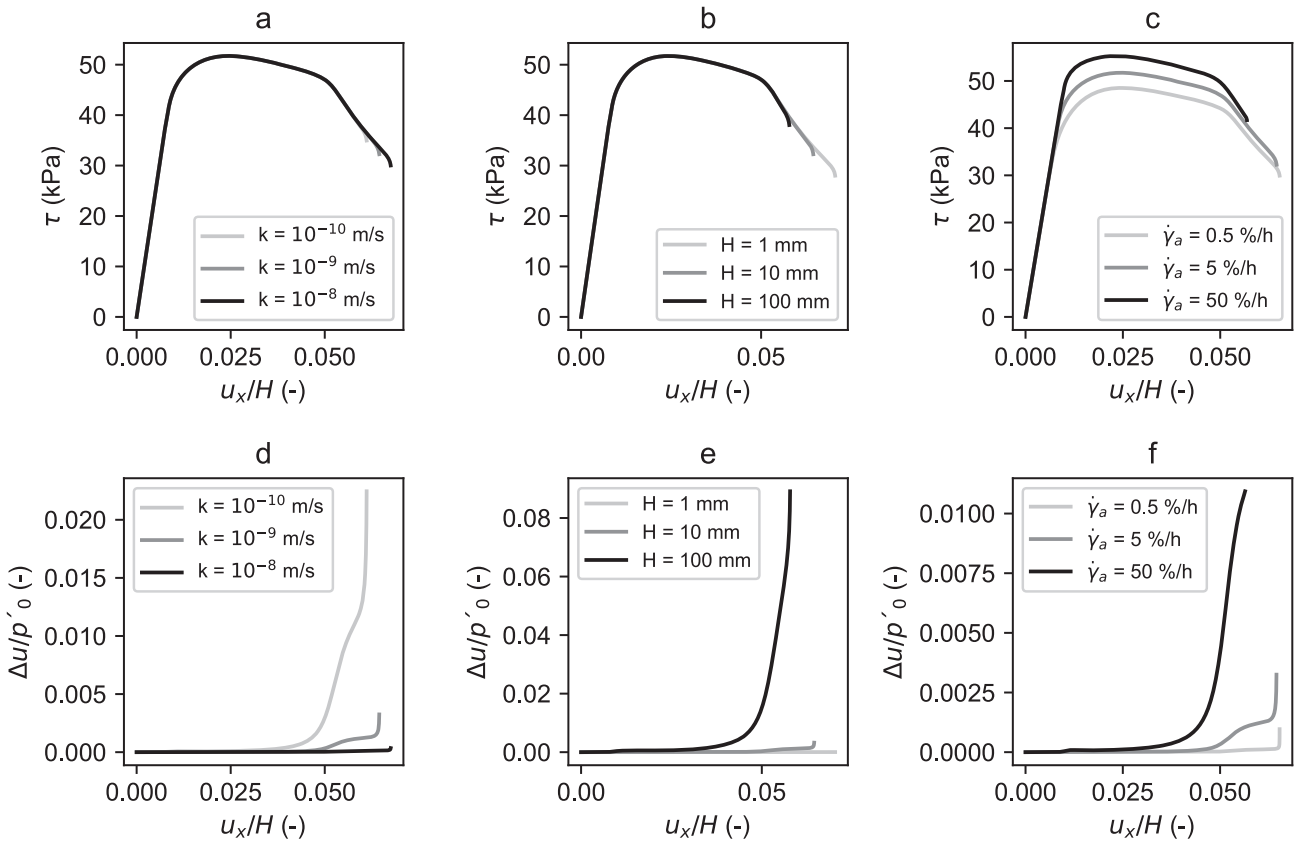

Fig. 17. Global response for columns with i/H = 0.2 and el/H = 0.002. a and d) varying k, constant: H = 10 mm, $\dot{\gamma}_a$ = 5 %/h. b and e) varying H, constant: k = 1e-9 m/s, $\dot{\gamma}$ = 5 %/h. c and f) varying $\dot{\gamma}_a$, constant: H = 10 mm, k = 1e-9 m/s.

solution exists that fulfils stress equilibrium and satisfies the applied displacement (eqn. (7)) simultaneously.

5.1.2. *Effect of increasing strain*

The applied constitutive model gives decreasing rate dependency in absolute terms (measured in kPa) at larger total strains, as demonstrated by the converging stress–strain curves for an element test with different constant strain rates in Fig. 6a. Rate dependency was implemented to the constitutive model by eqn. (5) and is reformulated in eqn. (8). In this formulation the logarithmic change in stress state (p'_{eq}/p'_m) is proportional to the logarithmic increase in strain rate ($\dot{\lambda}/\dot{\lambda}_{ref}$). The implication for the problem studied in this paper is that at larger total strains, a larger strain rate increase is necessary to achieve the same change in shear stress. This feature causes the increase in strain rate at the end of stage one softening and contributes to the rate increase at the end of stage two softening in Fig. 14.

$$\ln\left(\frac{\dot{\lambda}}{\dot{\lambda}_{ref}}\right) = \beta \cdot ln\left(\frac{p'_{eq}}{p'_m}\right) \tag{8}$$

For this constitutive model the decreasing rate dependency was partly a result of the model formulation using a fixed critical state line in p'-q space. Alternative formulations, for example using hyper-viscoplasticity (Grimstad et al., 2020; Grimstad et al., 2021) will result in non-unique critical state friction angle for different strain rates, meaning that the stress paths do not converge at large shear strains and hence makes it more difficult to localise the shear strains. Experimental evidence on the topic is limited, as shearing to critical state may require large strains that are not possible in standard laboratory tests. An alternative solution for the model formulation would be to include the third invariant of stress, which could enforce the same shear mobilisation even for different p', and hence could extend the regularised period.

Increasing brittleness is known to hinder regularisation for dynamic analyses (Wang et al., 1996). The Norwegian quick clay that has been considered in this paper is significantly more brittle than those used in studies by: Needleman, 1988, Oka, et al., 1995 and Jostad, et al. 2006. The constitutive model may therefore be able to provide a longer regularised response for less brittle soils.

5.2. *Pore water flow*

The effect of pore water flow made no significant difference to the global response during softening stage one, as demonstrated for different imperfection heights (Fig. 11), different permeabilities (Fig. 17a) and different column heights (Fig. 17b). All elements were undergoing strain softening during this stage (negative second order work in Fig. 12a), and thus the pore pressures inside and outside the imperfection were similar (Fig. 16 and Fig. 17d-e).

It is more difficult to draw general conclusions on the relative importance of pore water flow during softening stages two and three due to the interrelating processes of strain rate-dependency, excess pore pressure generation and pore water flow. However, it is apparent that the duration of stage two softening is significantly affected by pore water flow: Fig. 17. Also, the decreasing strain rate at the imperfection edge during softening stage two and the subsequent unloading in stage three (Fig. 14) are attributed to pore water flow out of the imperfection and into the surrounding unloading material.

To allow direct comparison of pore water flow with both the same boundary conditions and strain rates it was necessary to conduct analyses with different soil permeabilities: Fig. 17a and d. The results show that using a higher permeability delays the onset of mesh dependency: pore water flow from the shear band into the surrounding soil increases the effective stresses and thus the strength within the imperfection.

Similarly, numerical studies by Jostad et al. (2006) and Thakur (2011) on normally consolidated clays found that pore pressure dissipation only regularised to a given state along the softening curve, after which results became mesh dependent.

5.3. Shear band thickness

The presented simulations did not result in a shear band thickness independent of boundary conditions: the shear band thickness was first controlled by the imperfection height and then rapidly became mesh dependent. Various combinations of imperfection size, column height and permeability (Fig. 17) did not result in different shear band thicknesses. The deformations always concentrated in the height of a single element at the end of an analysis.

5.4. Application of findings to geotechnical problems

In real cases, the combined effects of the problem geometry, friction between different materials and other boundary conditions will naturally introduce variations in stress mobilisation within the soil body. Hence it will not be necessary to introduce artificial imperfections to trigger strain localisation.

For the problem investigated in this paper, the undrained shear strength was reduced by a third before results become mesh dependent: this period of regularised response is often sufficient to find the global instability condition for a real boundary value problem. The behaviour at large strains including calculation of run-out distance is another problem that generally is analysed by other formulations, for example BingClaw (Kim et al., 2019). The study of a 2D boundary value problem is a topic of future work for the authors.

Pore water flow may have a larger role in a real boundary value problem where the condition within the shear band may be closer to a drained state, and hence flow of pore water could further limit the strain localisation.

6. Conclusion

The objective of this study was to establish to what extent mesh independent results could be achieved by accounting for strain rate dependency and pore water flow. A constitutive model that replicated the laboratory test results of a soft sensitive clay was used to analyse a simple boundary value problem of a column of soil undergoing horizontal shear deformation.

It was shown that the model provides a period of mesh independent softening, but at larger strains the response becomes mesh dependent. The use of strain rate dependency prevents a shear band from forming immediately after peak by allowing the material inside and outside the imperfection to continue deforming at different rates. The response remains regularised even after the formation of a shear band, and it is demonstrated that pore water flow assists in prolonging the regularised response. It is therefore possible to achieve a regularised response for a strain-softening clay without the need to introduce an internal length scale, as for instance used in the non-local strain formulation. The one-dimensional shearing problem in this paper has been useful in allowing the identification and classification of the multiple softening stages and it provides the basis for further investigations in two dimensions.

CRediT authorship contribution statement

Laura Rødvand: Methodology, Validation, Formal analysis, Writing – original draft. **Hans Petter Jostad:** Supervision, Writing – review & editing. **Gustav Grimstad:** Software, Writing – review & editing. **Lars Andresen:** Supervision, Writing – review & editing.

Declaration of Competing Interest

The authors declare that they have no known competing financial interests or personal relationships that could have appeared to influence the work reported in this paper.

Acknowledgements

We thank Jon Rønningen for his assistance in implementing the constitutive model.

Funding

The main author gratefully acknowledges the STIPINST funding (nr. 259863) from the Research Council of Norway (RCN) and funding from the Norwegian Geotechnical Institute (NGI).

References

Berre, T., 1973. Effect of rate of strain of the stress-strain relationship for undrained triaxial tests on plastic Drammen clay. NGI report 50301-4.
de Borst, R., Duretz, T., 2020. On viscoplastic regularisation of strain-softening rocks and soils. Int. J. Numer. Anal. Meth. Geomech. 44 (6), 890–903. https://doi.org/10.1002/nag.3046.
Gens, A., Nova, R., 1993. Conceptual bases for a constitutive model for bonded soils and weak rocks. In: Geotechnical Engineering of Hard Soils – Soft Rocks. Rotterdam, pp. 485–494.
de Borst, R., Sluys, L.J., Muhlhaus, H.-B., Pamin, J., 1993. Fundamental issues in finite element analyses of localization of deformation. Eng. Comput. 10 (2), 99–121.
Graham, J., Crooks, J.H.A., Bell, A.L., 1983. Time effects on the stress-strain behaviour of natural soft clays. Géotechnique 33 (3), 327–340. https://doi.org/10.1680/geot.1983.33.3.327.
Grimstad, G., 2009. Development of effective stress based anisotropic models for soft clays. PhD thesis. Norwegian University of Science and Technology.
Grimstad, G., Degago, S.A., Nordal, S., Karstunen, M., 2010. Modeling creep and rate effects in structured anisotropic soft clays. Acta Geotech. 5 (1), 69–81. https://doi.org/10.1007/s11440-010-0119-y.
Grimstad, G., Long, M., Dadrasajirlou, D., Amiri, S.A.G., 2021. Investigation of development of the earth pressure coefficient at rest in clay during creep in the framework of hyper-viscoplasticity. Int. J. Geomech. 21 (1), 04020235. https://doi.org/10.1061/(ASCE)GM.1943-5622.0001883.
Grimstad, G., Dadrasajirlou, D., Ghoreishian Amiri, S.A., 2020. Modelling creep in clay using the framework of hyper-viscoplasticity. Géotechn. Lett. 10 (3), 404–408. https://doi.org/10.1680/jgele.20.00004.
Gylland, A., Long, M., Emdal, A., Sandven, R., 2013. Characterisation and engineering properties of Tiller clay. Eng. Geol. 164, 86–100. https://doi.org/10.1016/j.enggeo.2013.06.008.
Gylland, A.S., Jostad, H.P., Nordal, S., 2014. Experimental study of strain localization in sensitive clays. Acta Geotech. 9 (2), 227–240. https://doi.org/10.1007/s11440-013-0217-8.
Janbu, N., 1985. Soil models in offshore engineering. Géotechnique 35 (3), 241–281. https://doi.org/10.1680/geot.1985.35.3.241.
Jostad, H., Andresen, L., Thakur, V., 2006. Calculation of shear band thickness in sensitive clays. In: Numerical Methods in Geotechnical Engineering. Taylor & Francis, pp. 27–32. doi: 10.1201/9781439833766.ch4.
Karstunen, M., Krenn, H., Wheeler, S.J., Koskinen, M., Zentar, R., 2005. Effect of anisotropy and destructuration on the behavior of Murro test embankment. Int. J. Geomech. 5 (2), 87–97. https://doi.org/10.1061/(ASCE)1532-3641(2005)5:2(87).
Karstunen, M., Yin, Z.-Y., 2010. Modelling time-dependent behaviour of Murro test embankment. Géotechnique 60 (10), 735–749. https://doi.org/10.1680/geot.8.P.027.
Kim, J., Løvholt, F., Issler, D., Forsberg, C.F., 2019. Landslide material control on tsunami genesis—the Storegga slide and tsunami (8,100 Years BP). J. Geophys. Res. Oceans 124 (6), 3607–3627. https://doi.org/10.1029/2018JC014893.
Kulhawy, F.H., Mayne, P.W., 1990. Manual on Estimating Soil Properties for Foundation Design, EPRI.
Länsivaara, T., 1999. A Study of the Mechanical Behavior of Soft Clay. PhD thesis. Norwegian University of Science and Technology.
Leroueil, S., Kabbaj, M., Tavenas, F., Bouchard, R., 1985. Stress–strain–strain rate relation for the compressibility of sensitive natural clays. Géotechnique 35 (2), 159–180. https://doi.org/10.1680/geot.1985.35.2.159.
Loret, B., Prevost, J.H., 1991. Dynamic strain localization in fluid-saturated porous media. J. Eng. Mech. 117 (4), 907–922. https://doi.org/10.1061/(ASCE)0733-9399(1991)117:4(907).
Lunne, T., Andersen, K.H., 2007. Soft clay shear strength parameters for deepwater geotechnical design. In: Proceedings of the 6th International Off shore Site Investigation and Geotechnics Conference. London.
Mitchell, J.K., Soga, K., 2005. Fundamentals of Soil Behavior, third ed. Wiley.

Needleman, A., 1988. Material rate dependence and mesh sensitivity in localization problems. Comput. Methods Appl. Mech. Eng. 67 (1), 69–85. https://doi.org/10.1016/0045-7825(88)90069-2.

Oka, F., Kodaka, T., Kimoto, S., Ichinose, T., Higo, Y., 2005. Strain localization of rectangular clay specimen under undrained triaxial compression conditions. Soil Mech. Geotech. Eng.: Geotechnol. Harmony Global Environ. 2, 841–844. https://doi.org/10.3233/978-1-61499-656-9-841.

Oka, F., Adachi, T., Yashima, A., 1995. A strain localization analysis using a viscoplastic softening model for clay. Int. J. Plast. 11 (5), 523–545.

Rezania, M., Taiebat, M., Poletti, E., 2016. A viscoplastic SANICLAY model for natural soft soils. Comput. Geotech. 73, 128–141. https://doi.org/10.1016/j.compgeo.2015.11.023.

Schofield, A., Wroth, C., 1968. Critical state Soil Mechanics. McGraw-Hill, London.

Schrefler, B.A., Majorana, C.E., Sanavia, L., 1995. Shear band localization in saturated porous media. Arch. Mech. 47 (3), 577–599.

Sluys, L.J., de Borst, R., 1992. Wave propagation and localization in a rate-dependent cracked medium—model formulation and one-dimensional examples. Int. J. Solids Struct. 29 (23), 2945–2958. https://doi.org/10.1016/0020-7683(92)90151-I.

Soga, K., Mitchell, J.K., 1996. Rate-dependent deformation of structured natural clays. In: Sheahan, T.C., Kaliakin, V.N. (Eds.), Measuring and Modeling Time Dependent Soil Behavior. ASCE, Washington, pp. 243–257.

Thakur, V., 2011. Numerically observed shear bands in soft sensitive clays. Geomech. Geoeng. 6 (2), 131–146. https://doi.org/10.1080/17486025.2010.546434.

Thakur, V., Nordal, S., Viggiani, G., Charrier, P., 2018. Shear bands in undrained plane strain compression of Norwegian quick clays. Can. Geotech. J. 55 (1), 45–56. https://doi.org/10.1139/cgj-2016-0443.

Tornborg, J., Karlsson, M., Kullingsjö, A., Karstunen, M., 2021. Modelling the construction and long-term response of Göta Tunnel. Comput. Geotech. 134, 104027. https://doi.org/10.1016/j.compgeo.2021.104027.

Wang, W.M., Sluys, L.J., De Borst, R., 1996. Interaction between material length scale and imperfection size for localisation phenomena in viscoplastic media. Eur. J. Mech., A/Solids 15 (3), 447–464.

Yesuf, G.Y., 2008. Behavior of Norwegian Quick Clays under Varying Strain Rates. Norwegian University of Science and Technology.

Yin, Z.Y., Karstunen, M., 2011. Modelling strain-rate-dependency of natural soft clays combined with anisotropy and destructuration. Acta Mech. Solida Sin. 24 (3), 216–230. https://doi.org/10.1016/S0894-9166(11)60023-2.